Korean J. Chem. Eng., **26**(1), 250-257 (2009)

Electrochemical characteristics of Al-Mg alloy in seawater for leisure ship: Stress corrosion cracking and hydrogen embrittlement

Seong-Jong Kim†, Min-Su Han, and Seok-Ki Jang

Division of Marine Engineering, Mokpo Maritime University, 571, Jukgyo-dong, Mokpo-si, Jeonnam 530-729, Korea
(*Received 27 December 2007 • accepted 26 June 2008*)

Abstract−We investigated the mechanical and electrochemical properties of aluminum alloys. Aluminum alloys do not corrode due to the formation of an anti-corrosive passive film, such as Al_2O_3 or $Al_2O_3 \cdot 3H_2O$, which resists corrosion in neutral solutions. In seawater, however, Cl^- ions destroy this passive film. The current density in the first passivity range during the application of anodic protection had a similar value as that for concentration polarization by dissolved oxygen during the application of cathodic protection. The current density in the first passivity range had the lowest value overall. The lowest current densities in the potentiostatic and galvanostatic tests occurred at potentials of −1.4 to −0.7 V and −0.9 to −0.7 V, respectively.

Key words: Electrochemical Property, Aluminum Alloy, Corrosion, Seawater, Passivity, Cathodic Protection, Potentiostatic Test

INTRODUCTION

Fiber-reinforced plastic (FRP) ships, including small fishing boats, have many environmental and recycling problems. For example, no suitable method exists for decommissioning an FRP ship. If Al were used as a substitute for FRP in ships and boats, the result would be more environmentally friendly vessels that are easy to recycle and have the added value of reduced fuel consumption, higher speed, and increased load capacity [1-3]. The composite FRP materials of which they are constructed are susceptible to fire and are prohibited from use in high-speed passenger ships and cargo boats with gross tonnages in excess of 500 tons, such as those commonly used in coastal navigation. In addition, FRP ships are small. As with wooden vessels, larger craft cannot detect FRP ships by radar since their composite materials reflect radar waves poorly [4-6]. According to data collected by the Ministry of Maritime Affairs and Fisheries, a large proportion of ship accidents involve these vessels, comprising 72.4% of all marine accidents between 1998 and 2002 and approximately 58% of all collisions involving fishing boats [7]. In light of these considerations, aluminum offers a far better material for ship building than does FRP. It is environmentally friendly, easy to recycle, and provides a high added value to fishing boats. Aluminum craft require less fuel. Developed nations have shown an increasing interest in utilizing Al alloys in ships since environmental restrictions on scrapping FRP ships have become stronger [8].

We evaluated the electrochemical stress corrosion cracking and hydrogen embrittlement characteristics of 5083-H112 Al alloy specimens in seawater. Our results can be used as reference data for ship design.

MATERIALS AND EXPERIMENTAL DESCRIPTION

The main additional element of an Al-Mg alloy (5XXX series) is Mg. Al-Mg alloys are not heat treated, and have high strength and good welding properties. They are often used as materials for high-pressure vessels, ships, and other marine structures because they have good corrosion resistance in seawater environments. Al-Mg alloys include 5005, 5050, 5052, 5652, 5082, 5083, 5086, 5154, 5254, 5454, 5456, and 5N01 [9]. Table 1 shows the mechanical properties and chemical composition of the 5083-H112 Al alloy.

The 5083-H112 Al alloy specimens used for the electrochemical tests were mounted with epoxy resin to give an exposed area of 100 mm^2, and then polished with #600 emery paper. The specimens were carefully degreased with acetone and water, and the corrosion potential was measured over 86,400 s in natural seawater. The polarization system consisted of a Pt coil, which acted as a counter electrode, and a Ag/AgCl saturated KCl reference electrode. The tests were carried out at a scan rate of 2 mV/s at room temperature. Anodic and cathodic polarization were created from an open-circuit potential to +3.0 and 2.0 V using a Ag/AgCl electrode (SSCE).

In the potentiostatic tests, a variety of polarization potentials in seawater were applied for 1,200 s and evaluated in terms of the variations in current density with time and by ascertaining the current density remaining after 1,200 s at the applied potential. The degree of corrosion was analyzed under a scanning electron microscope (SEM) following the tests.

In the galvanostatic tests, a variety of current densities were applied in seawater for 5,400 s and the resulting specimen surface morphologies were evaluated with the SEM. Tafel analyses were performed under both anodic and cathodic conditions from the optimum cathode protection (OCP) up to ±0.25 V with aeration. The corrosion potential and corrosion current density were determined from the Tafel analytical results by comparison with various reference specimens.

RESULTS AND DISCUSSION

Fig. 1 shows the potential variation over a period of 86,400 s for a 5083-H112 Al specimen in a natural seawater solution. In the early

†To whom correspondence should be addressed.
E-mail: ksj@mmu.ac.kr

Table 1. Comparison of chemical composition and mechanical properties for 5083-H112

(a) Chemical composition (%)

	Si	Fe	Cu	Mn	Mg	Cr	Zn	Ti	Al
5083-H112	0.103	0.271	0.018	0.637	4.427	0.098	0.008	0.028	Bal.

(b) Mechanical properties

	Tensile strength (MPa)	Yield strength (MPa)	Elongation (%)
5083-H112	318.6	164.3	23.74

stages of immersion, the corrosion potential of the Al alloy shifted abruptly in the more noble direction with the formation of a film in the seawater. The highest potential, which occurred 2,000 s after immersion, was −0.78 V; thereafter, the potential decreased at regular intervals. A passive film formed at 12,500 s, but was destroyed by the action of the Cl^- in the seawater. The potential shifted to the active direction until 20,000 s, after which the formation and destruction of the passive film was repeated. The potential after 40,000 s stabilized for a period of time, but after 50,000 s, the potential started to increase slowly to −0.96 V at the end of the test.

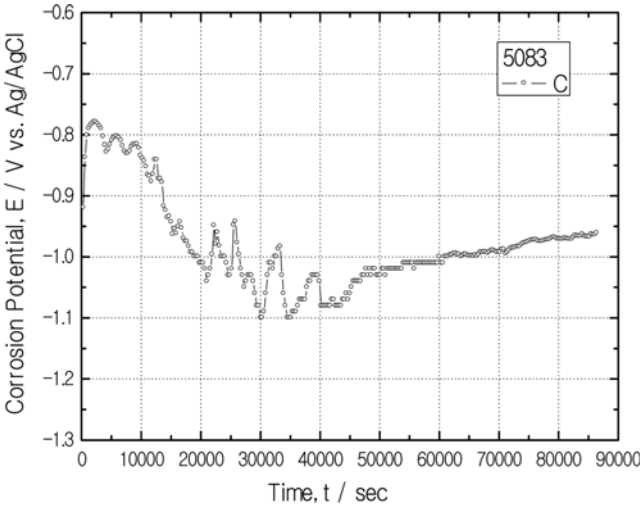

Fig. 1. Variation of potential for 5083-H112 specimen in natural sea water solution.

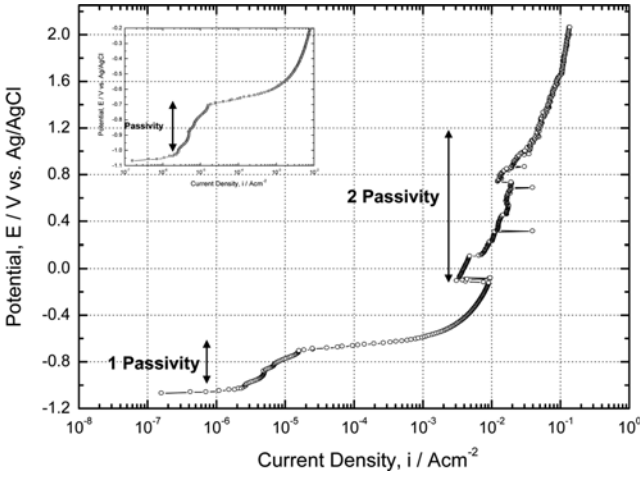

Fig. 2. Anodic polarization curves in natural sea water solution.

Fig. 2 shows the anodic polarization curve for a 5083-H112 Al specimen in seawater. The first passivity phenomenon occurred at a potential of −1.0 to −0.7 V. However, the current density increased markedly above −0.7 V as the passivity film was destroyed. Thereafter, the current density decreased as the second passivity film formed at −0.1 V. After this, the current density slowly increased with time and then decreased above 0.7 V. The current density increased when the second passivity film was completely formed above 1.2 V. Therefore, the second passivity range did not provide corrosion protection due to the high current density. In general, Al and Al alloys do not corrode in neutral solutions due to the formation of a film such as Al_2O_3 and $Al_2O_3 \cdot 3H_2O$ [10]. However, in seawater, the passive films formed during anodic polarization are subsequently destroyed by the Cl^- in the solution; the passivity continues to develop due to the self-healing capacity of Al. In previous investigations [6,11], the current density of the 5456 alloy decreased abruptly at a potential of −0.3 to 0.4 V, while the current density of the 7075 alloy increased with the potential during anodic polarization without passivity developing. The current density of the 5456 alloy remained less than that of the 1050 alloy. A passivity phenomenon was not observed in the 7075 alloy; instead, a continuous increase in current density occurred. This alloy was weakened by stress corrosion cracking, and the 1050 alloy proved to be superior to the 7075 alloy in this respect. However, the 1050 alloy is too weak for building ships, whereas the 5456 alloy is widely used because it is both strong and resistant to stress corrosion cracking in seawater environments. The stress corrosion cracking characteristics of all specimens is best analyzed by using anodic polarization curves.

Fig. 3 gives the results of the cathodic polarization tests for 5083-H112 Al specimens in seawater. The polarization trend for the alloy shows the effects of concentration polarization due to oxygen reduction ($O_2+2H_2O+4e^- \rightarrow 4OH^-$) and activation polarization due to hydrogen generation ($2H_2O+2e \rightarrow H_2+2OH^-$). The potential that generated the concentration polarization, or the corrosion protection potential, from the cathodic polarization curve ranged from −0.86 to −1.55 V. The current density of the protection potential was 10^{-6} to 10^{-4} A/cm^2. However, the potential for the first passivity phenomenon from the anodic polarization curve was −1.0 to −0.7 V, corresponding to a current density of 2.5×10^{-6} to 1.7×10^{-5} A/cm^2. Therefore, the optimum protection potential is in the first passivity range. If the potential is not controlled accurately during the anodic protection, a danger exists of stress corrosion cracking due to the active dissolution reaction. We also investigated if improvements to the corrosion resistance could be obtained when Al is subjected to friction stir welding to relieve the residual stress due to heat. Upon close examination, anodic protection of friction stir welding on a 1050

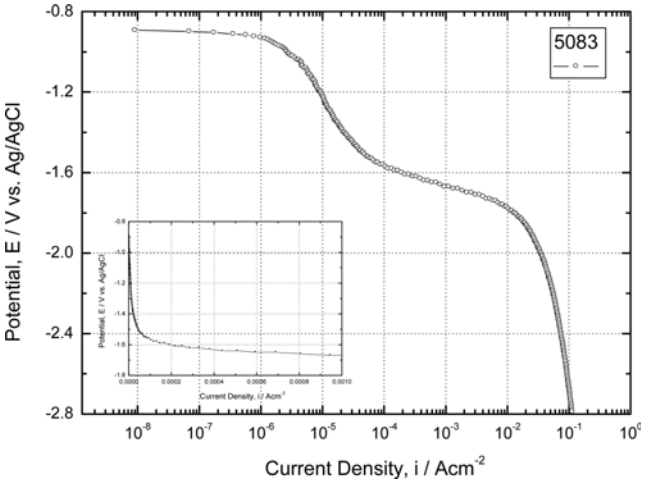

Fig. 3. Cathodic polarization curves in natural sea water solution.

alloy specimen was more economical than cathodic protection [12]. In investigations of hydrogen embrittlement in high-strength steel [13-17], the point at which the crossover takes place from concentration polarization due to oxygen reduction to activation polarization due to hydrogen generation is approximately −1,000 mV (SCE). This gives crossover points for the 1050, 5456, and 7075 alloys at approximately −1.66, −1.7, and −1.64 V, respectively. The 5456 alloy has the lowest potential, while the 7075 alloy has the highest, which indicates that the 7075 alloy is most affected by hydrogen embrittlement. During the polarization tests for the 5456-H116 Al alloy, the destruction and formation of the passivity film in the anodic polarization curve were repeated [6,11]. The current density at the potential that generated hydrogen gas increased abruptly in the cathodic polarization curve.

Fig. 4 shows the time-current density curves obtained from a potentiostatic analysis of the 5083-H112 Al alloy in seawater. A variation in the current density was observed over the entire 1,200 s of the experiment between 0 and −1.2 V (see Fig. 4(a)), but the values remained high, as shown in Fig. 2. The current density increased with the applied potential. In the potentiostatic tests under three applied potential conditions, the current density remained at a high value from the early stages until the end of the tests. The current density was also high along with the potential during anodic polarization due to the active dissolution reaction. Fig. 4(b) shows the potentiostatic results for the range −0.7 to −0.4 V. The current densities at applied potentials of −0.4 and −0.6 V remained stable from the earliest stages of the tests. A high current density was observed in the initial stages, and this trend was maintained to the end of the tests. However, the current density for an applied potential of −0.7 V was low since this range corresponds to the first passivity section. Fig. 4(c) depicts the potentiostatic results for the range −0.9 to −0.8 V. In the early stages, the current density at −0.9 V was 1×10^{-5} A/cm^2. This value slowly decreased with time, and the current density exhibited a continuous hunting phenomenon over the range 2×10^{-6} to 3×10^{-6} A/cm^2 until the end of the tests. The current densities were low since both conditions occurred in the first passivity range.

Fig. 5 compares the current densities obtained from the potentiostatic tests after 1,200 s for all 5083-H112 Al specimens analyzed at various anodic potentials in natural seawater. Each potentiostatic test was executed several times; the black circles represent the mean values. The current densities for the range −0.9 to −0.7 V had similar low values for all tests since they fell in the first passivity range. The current density increased with the potential at −0.6 V. Above −0.4 V, the current densities increased considerably with the potential. The current density obtained after the potentiostatic

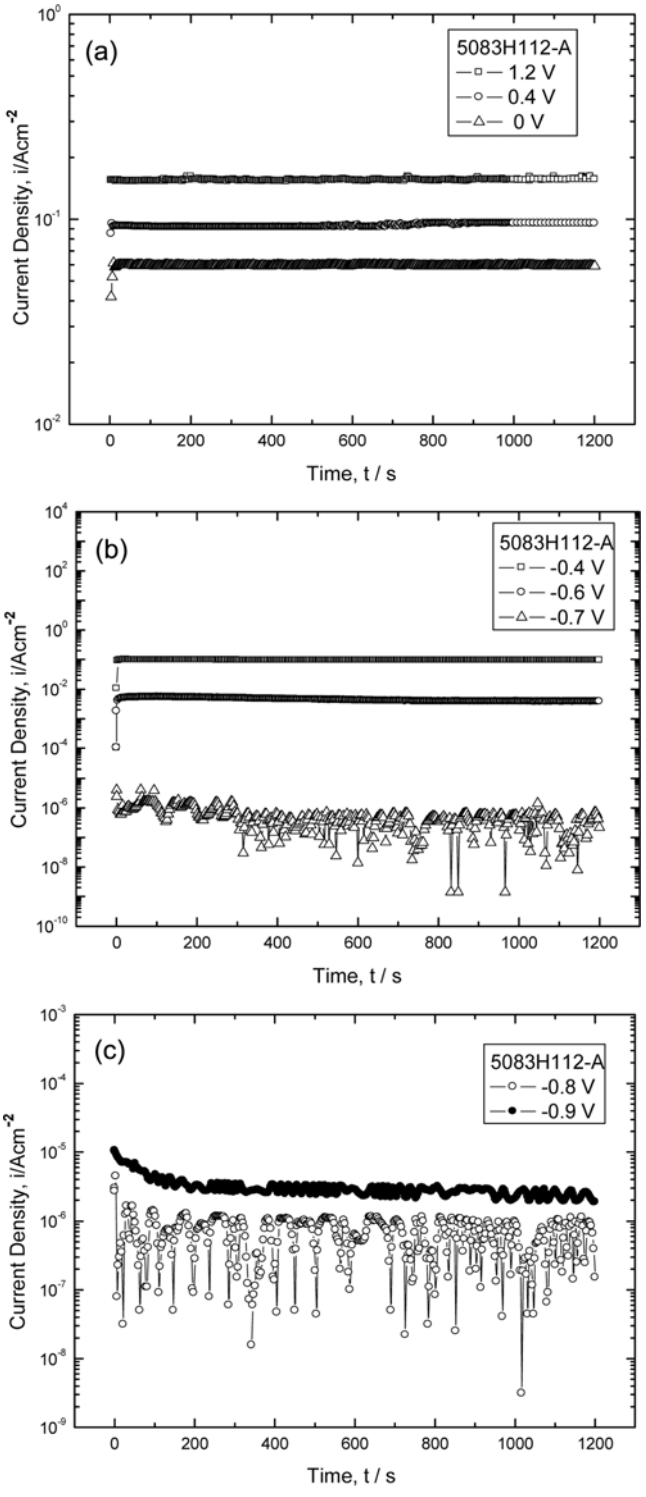

Fig. 4. Time-current density curves during potentiostatic experiment for 5083-H112 specimen in natural sea water solution.

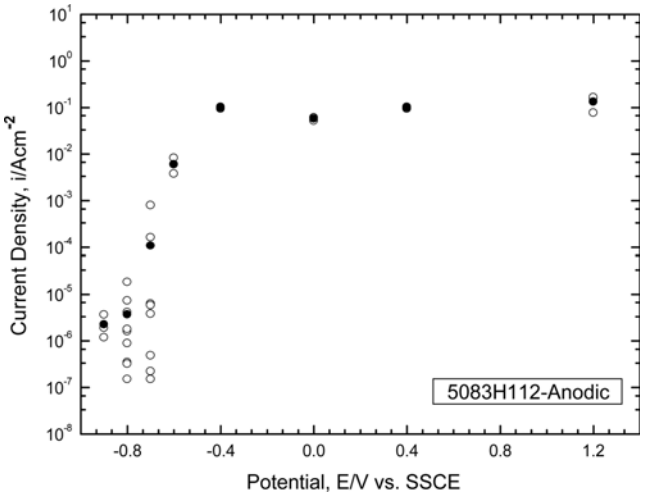

Fig. 5. Time-current density curves during potentiostatic experiment at various anodic potential for 5083-H112.

tests at an applied potential of 0 V was lower than that obtained at −0.4 V, notwithstanding the high potential due to the second passivity section. The current densities obtained above 0 V had high values. These trends were similar to those observed during anodic polarization.

Fig. 6 shows the time-current density curves of the potentiostatic tests between −1.5 and −1.0 V for the 5083-H112 Al specimens in seawater, a potential range that includes dissolved oxygen reduction, i.e., the protection potential range. Fig. 6(a) gives the results at applied potentials of −1.2 to −1.0 V. The current densities between −1.2 and −1.0 V became stable around 200 s, with values at 1,200 s of 5.0386×10^{-6}, 1.1261×10^{-5}, and 1.155×10^{-6} A/cm^2 at −1.0, −1.1, and −1.2 V, respectively. All current densities tended to be low stable values since they fell within the protection potential range. A higher current density indicates an increasing potential in the active direction. Generally, this trend is similar to cathodic behavior. The results of the potentiostatic tests between −1.35 and −1.25 V are shown in Fig. 6(b). Unlike between −1.2 and −1.0 V, the current densities for −1.35 to −1.25 V were stable in the early stages of the tests. This trend was also observed in the cathodic polarization curve. A high current density indicates an increasing potential in the negative direction. Fig. 6(c) shows the results at applied potentials of −1.5 to −1.4 V. The current densities were stable throughout the tests at applied potentials of −1.5 and −1.4 V. However, the current density at −1.45 V started at a low value and then gradually increased to give a high value after 1,200 s.

Fig. 7 shows the time-current density curves from the potentiostatic tests between −2.4 and −1.55 V for the 5083-H112 Al specimens in seawater. The results of potentiostatic tests for between −1.7 and −1.55 V, which spans the crossover from concentration polarization to activation polarization, are shown in Fig. 7(a). The current densities at −1.7 to −1.55 V increased over the first 100-400 s, and remained stable thereafter. This range corresponded to the concentration polarization for the cathodic polarization curve. High current densities were obtained in the potentiostatic tests. After 1,200 s, the current densities were 0.00242, 0.00466, and 0.01109 A/cm^2 for applied potentials of −1.55, −1.60, and −1.70 V, respectively. Even

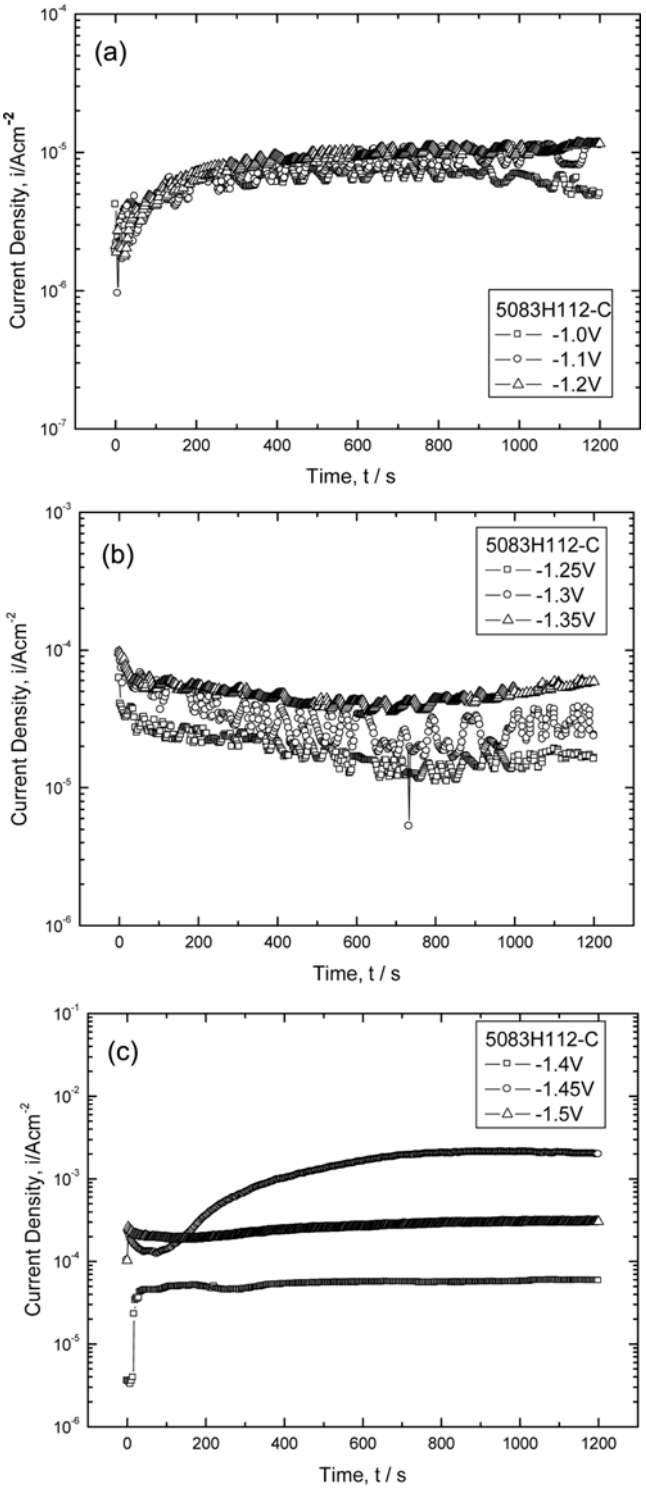

Fig. 6. Time-current density curves during potentiostatic experiment at range of −1.5 V~−1.0 V for 5083-H112 specimen in natural sea water solution.

though the current density at −1.55 V was within the protection potential range, it was slightly elevated at 0.00242 A/cm^2 during anodic polarization, possibly due to the monatomic reaction of hydrogen ions ($H^+ + e \rightarrow H$) prior to activation polarization. The current density increased as the potential shifted to a more negative value. This

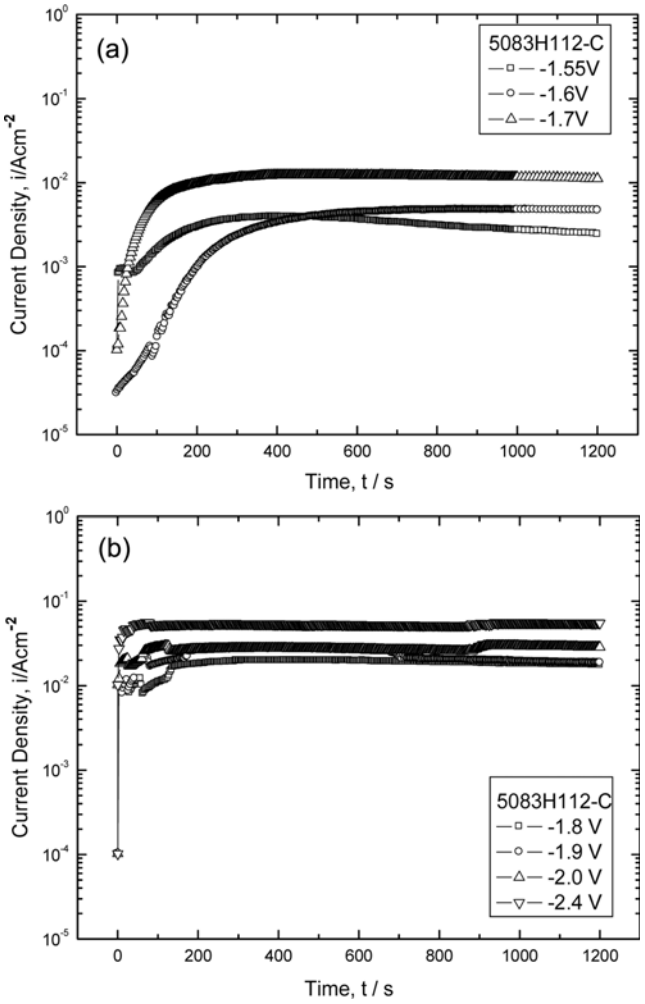

Fig. 7. Time-current density curves during potentiostatic experiment at range of –2.4 V~–1.55 V for 5083-H112 specimen in natural sea water solution.

potential range corresponded to the generation of atomic hydrogen ($H^+ + e \rightarrow H$) or the production of molecular hydrogen from atomic hydrogen ($H^+ + e + H \rightarrow H_2$, $H + H \rightarrow H_2$), resulting in the acceleration of activation polarization and an increase in the current density [6, 11]. We concluded that atomic hydrogen affected the potential at which the crossover occurred. Fig. 7(b) shows the potentiostatic results for between −2.4 and −1.8 V. The current density increased linearly with increases in negative potential. The activation polarization intensified the generation of hydrogen due to cathodic polarization, which could be seen by the unaided eye. The effect of atomic hydrogen was less than that of molecular hydrogen.

A comparison of the current densities measured for the 5083-H112 Al alloy in seawater at the conclusion of each potentiostatic test at 1,200 s is shown in Fig. 8 for various cathodic potentials. The potential between −1.4 and −1.0 V during cathodic polarization had a low current density, which indicated corrosion protection. At −1.45 V, the effects of atomic hydrogen appeared in the elevated current density. A potential of −1.55 V corresponded to the crossover from dissolved oxygen reduction to the activation reaction, and was influenced by the presence of both atomic and molecular hydrogen

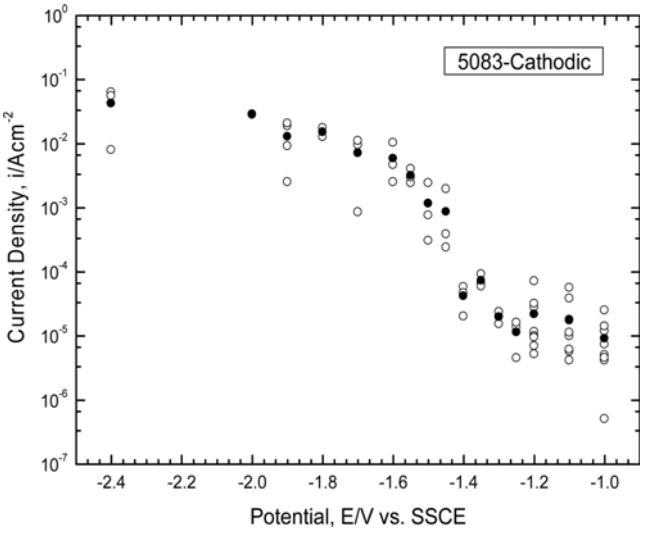

Fig. 8. Comparison of current density after potentiostatic experiment of 1,200 s for 5083F specimen at various cathodic potential in natural sea water solution.

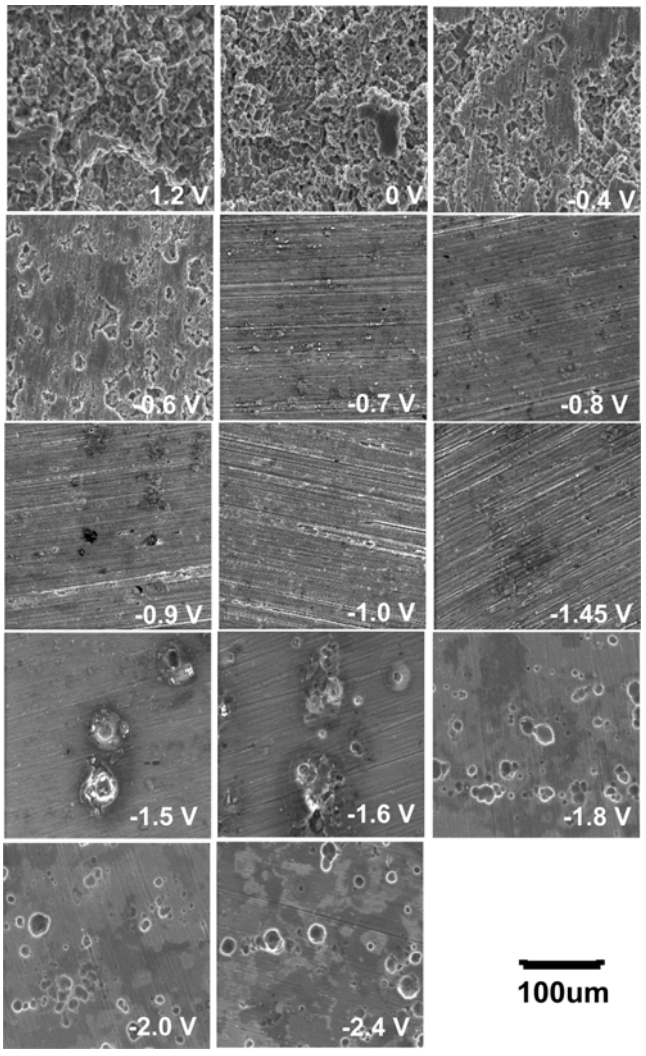

Fig. 9. Surface morphologies of specimen after potentiostatic experimentduring 1,200 s at −1.45 V~1.2 V in natural sea water.

[13,14]. We concluded, however, that effects on the current density due to atomic hydrogen were small. Current densities between −1.45 and −2.4 V increased abruptly with any shift toward the active direction, and it seems likely that their high current densities reflected the presence of molecular hydrogen. This was the same trend observed in cathodic polarization.

Fig. 9 shows the surface morphologies of the specimens after the 1,200-s potentiostatic tests for a potential of −2.4 to 1.2 V in natural seawater. The surface morphology at −0.4 V, the potential above the first passivity range, indicated corrosion due to the active dissolution reaction. However, parts of the surface were not corroded. The current density at an applied potential of 0 V decreased due to the second passivity phenomenon, although the active dissolution reaction occurred. We verified that the dissolution reaction on the specimen surface progressed with increasing applied potential. The surface morphologies at high applied potentials were not observed due to the high current densities and long application times.

An applied potential of −0.6 V corresponds to the increase in the current density with potential after the first passivity range. The surface morphology at −0.6 V was similar to that at −0.4 V; however, the dissolution reaction at −0.6 V was slower than that at −0.4 V. This trend coincided with the anodic polarization curve. The surface morphologies for −0.9 to −0.7 V had very little corrosion since this potential range corresponded to the first passivity phenomenon. The potential between −1.45 and −1.0 V generated concentration polarization due to the dissolved oxygen reduction reaction of the cathodic polarization curve. This potential range corresponds to the protection potential during cathodic protection. Some dissolution reaction at this potential range was observed around the scratches formed during the polishing process, but very little specimen damage occurred overall. The potential between −1.7 and −1.5 V corresponds to the crossover point between concentration polarization due to oxygen reduction and activation polarization due to hydrogen generation. An applied potential of −1.5 V corresponds to concentration polarization. Specimen damage was observed due to the monatomic reaction of hydrogen ions ($H^+ + e \rightarrow H$), but hydrogen gas generation was not observed during the test. For a potential of −1.7 to −1.55 V, hydrogen gas was observed with the potential prominently shifting in the negative direction, resulting in specimen damage due to activation polarization from the hydrogen gas. In these tests, hydrogen gas was observed with the naked eye. Considerable hydrogen gas was generated due to the effect of molecular hydrogen for the potential between −2.4 and −1.8 V, resulting in specimen damage.

The current density increased when the applied potential shifted in the negative direction, resulting in a wide range of specimen damage. However, the high current densities remained relatively constant. In a previous investigation [6], the current density increased suddenly when the applied potential shifted beyond the protection potential range in either the anodic or cathodic directions. The high-strength 7075 alloy had the highest current densities. This alloy is most prone to stress corrosion cracking and hydrogen embrittlement because the residual stress is high, which gives a high strength but also increases the hardness compared to the 1050 and 5456 alloys. In comparison, the 5456 alloy is less prone to stress corrosion cracking and hydrogen embrittlement in seawater due to its low current density [11]. The current density of the 7075 alloy was high compared to the 1050 and 5456 alloys. The optimum protection potential from −1.5 to −0.68 V for the 5456 alloy was obtained between −0.70 and −1.3 V, when the current densities were low. According to the U.K. criteria for cathodic protection (CP 1021), the protection potential of Al is −0.85 to −1.1 V (SSCE), and pitting does not occur at a cathodic polarized potential of about 0.15 V compared to the OCP [18]. The potential measurement tests conducted over a 24-h period in this study at potentials between −0.69 and −0.72 V agreed with the U.K. cathodic protection criteria for the 1050 alloy since the current densities remained low at all potentials. This is the principal reason for the low residual stress of the 1050 Al alloy.

Fig. 10 shows Tafel analyses for the 5083-H112 Al specimens in a natural seawater solution. The Tafel tests were performed several times, and the results gave similar overall trends. The corrosion potential and corrosion current density for the 5083-H112 Al specimen ranged from −0.5099 to −0.4362 V and 4×10^{-6} to 5.5×10^{-6} A/cm^2, respectively. The specimens showed excellent corrosion resistance in the seawater environment. Table 2 lists the results of the Tafel analyses in detail.

Fig. 11 presents the surface morphologies of the specimens observed under the SEM following the galvanostatic tests to compare the degree of corrosion for various current densities in natural seawater. In the early stages of the tests, dissolution reactions due to corrosion of the specimen in the seawater solution were observed around the scratches formed by the polishing process. These reactions pro-

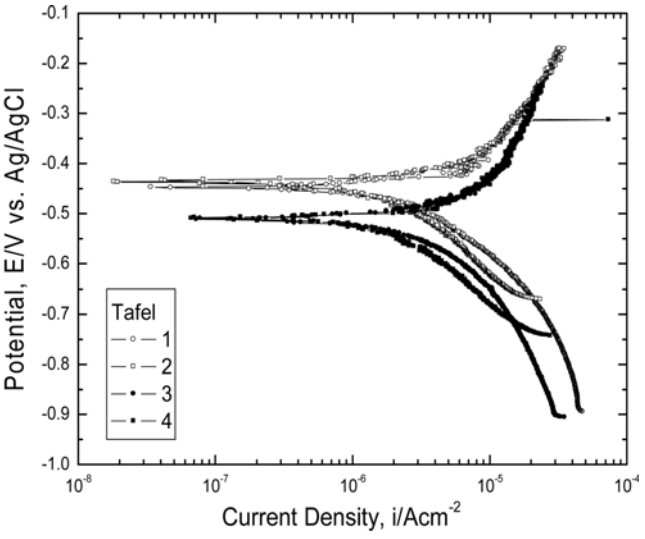

Fig. 10. Tafel analysis for 5083-H112 in natural sea water solution.

Table 2. Results obtained from Tafel analysis of 5083-H112 Al alloy in seawater

	Corrosion potential (V)	Corrosion current density (A/cm^2)
1	−0.4475	4×10^{-6}
2	−0.4362	5.5×10^{-6}
3	−0.5098	5.5×10^{-6}
4	−0.5099	4×10^{-6}
Average	−0.4759	4.75×10^{-6}

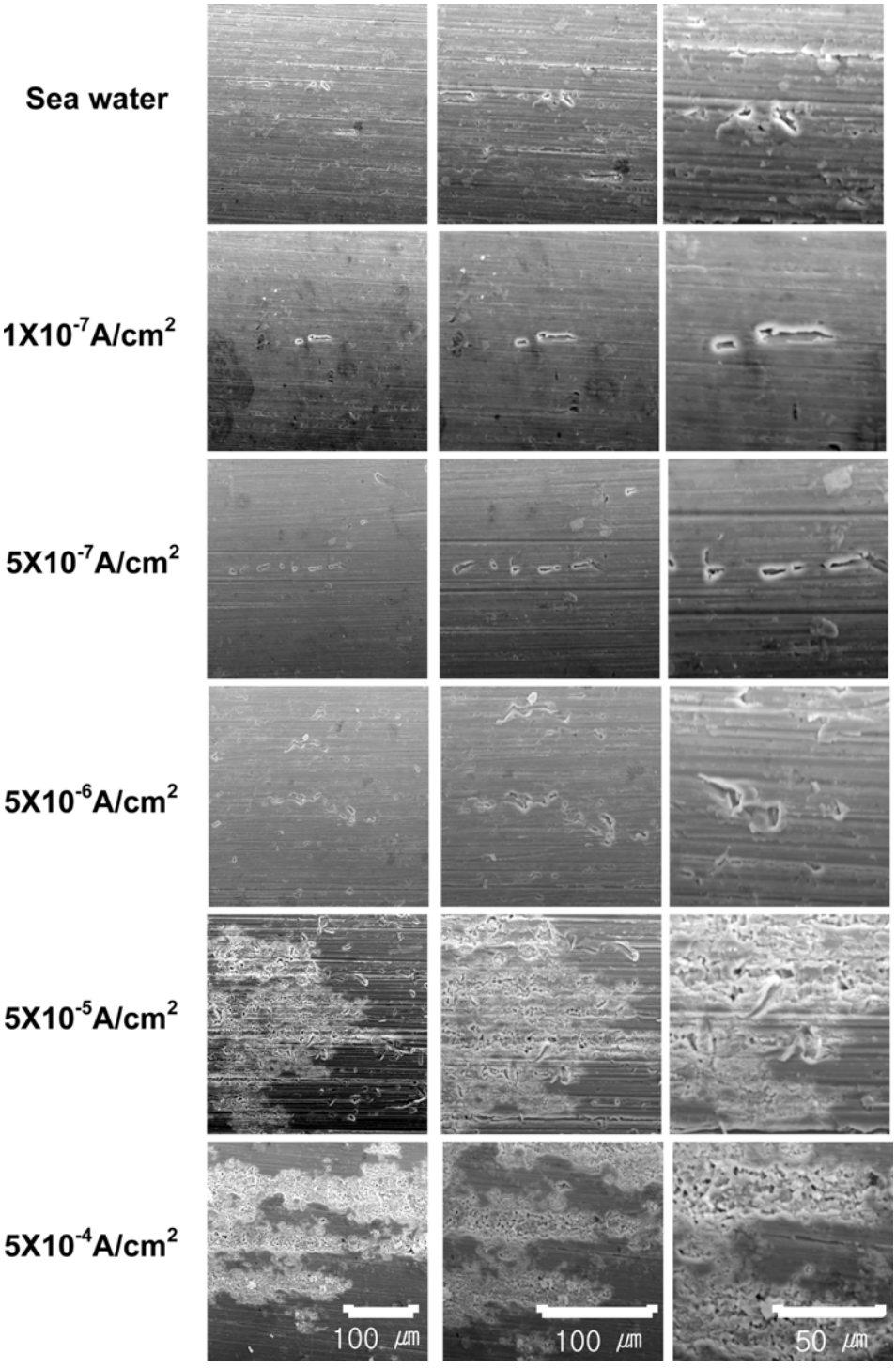

Fig. 11. Surface morphologies of specimen after galvanostatic experimental at various current density in natural sea water.

gressed with time. Similar low corrosion trends compared to natural seawater were observed for current densities of 1×10^{-7} and 5×10^{-7} A/cm^2. However, the surface morphology in the galvanostatic test with a current density of 5×10^{-6} A/cm^2 was similar to that under natural seawater conditions, but the corrosion was more widely distributed. The corrosion current density obtained from the Tafel analysis in seawater solution (4.75×10^{-6} A/cm^2) was less than 5×10^{-6} A/cm^2. Therefore, we concluded that degree of corrosion was small. However, active reactions were observed for applied current densities of 5×10^{-5} to 5×10^{-4} A/cm^2, unlike natural seawater conditions. A dissolution reaction was also observed simultaneously. The degree of corrosion was high with increasing current density, but the degree of corrosion remained low until the current density reached 5×10^{-6} A/cm^2. From the potentiostatic test results at 1,200 s, the potential range that gave a low current density of 5×10^{-6} A/cm^2 was -0.9 to -0.7 V, similar to results of the Tafel analyses. Therefore, the opti-

mum protection potential was between −0.9 and −0.7 V.

CONCLUSIONS

The results of our electrochemical experiment for the Al-Mg alloy (5083-H112) in seawater were as follows.

The polarization trend for the 5083-H112 Al alloy showed the effects of concentration polarization due to oxygen reduction (O_2+ $2H_2O+4e^- \rightarrow 4OH^-$) and activation polarization due to hydrogen generation ($2H_2O+2e \rightarrow H_2+2OH^-$). The crossover point between the two reactions was −1.55 V. The dissolved oxygen reduction reaction corresponded to the corrosion protection potential of − 1.55 V.

The current density in the first passivity range during the application of anodic protection had a similar value as that for concentration polarization by dissolved oxygen during the application of cathodic protection. The current density in the first passivity range had the lowest value overall.

The lowest current densities in the potentiostatic and galvanostatic tests occurred at potentials of −1.4 to −0.7 V and −0.9 to −0.7 V, respectively.

We concluded that the optimum protection condition was −0.9 to −0.7 V, corresponding to the first passivity range, by comparing the degree of surface corrosion after the galvanostatic tests.

REFERENCES

1. S. J. Kim and J. Y. Ko, International welding/joining conference-2007 (IWJC-Korea 2007), Seoul, Korea (2007).
2. S. J. Kim, J. Y. Ko and J. I. Kim, International welding/joining conference-2007 (IWJC-Korea 2007), Seoul, Korea (2007).
3. S. J. Kim and J. Y. Ko, International welding/joining conference-2007 (IWJC-Korea 2007), Seoul, Korea (2007).
4. S. J. Kim and J. Y. Ko, *Korean Journal of Marine Engineering*, **30**(1), 157 (2006).
5. S. J. Kim, *Materials Science Forum*, **510-511**, 158 (2006).
6. S. J. Kim and J. Y. Ko, *Korean J. Chem. Eng.*, **23**, 847 (2006).
7. J. H. Cho, *Korea Research Institute of Medium and Small Shipbuilding*, **10**(6), (2004).
8. Sky Al products corporation, *Journal of Japan Institute of Light Metals Welding*, **41**(11), 544 (2003).
9. Korea Register, *Material and Welding*, **2**(79), (2004).
10. M. Pourbaix, *Atlas of electrochemical equilibria*, NACE, 168-176 (1974).
11. S. J. Kim, J. Y. Ko and M. S. Han, *Korean J. Chem. Eng.*, **23**, 1028 (2006).
12. S. K. Jang, D. C. Lee, S. J. Kim, J. I. Jeon and S. H. Kim, *Proceedings of Marine Engineering Conference*, 139 (2004).
13. S. J. Kim and K. M. Moon, *Metals and Materials International*, **8**(4), 395 (2002).
14. S. J. Kim and K. M. Moon, *Metals and Materials International*, **8**(4), 387 (2002).
15. S. J. Kim, M. Okido and K. M. Moon, *Korean J. Chem. Eng.*, **20**, 560 (2003).
16. S. J. Kim, M. Okido and K. M. Moon, *Surface and Coatings Technology*, **169-170**, 163 (2003).
17. K. M. Moon, M. H. Lee, K. J. Kim and S. J. Kim, *Surface and Coatings Technology*, **169-170**, 675 (2003).
18. D. H. Jeon, *Control of corrosion and protection*, 316, Il-Joong publishing Co. (1985).